

LACK OF INFLATED RADII FOR *KEPLER* GIANT PLANET CANDIDATES RECEIVING MODEST STELLAR IRRADIATION

BRICE-OLIVIER DEMORY AND SARA SEAGER

Department of Earth, Atmospheric and Planetary Sciences, Massachusetts Institute of Technology, 77 Massachusetts Ave., Cambridge, MA 02139, USA; demory@mit.edu

Received 2011 August 29; accepted 2011 October 11; published 2011 November 2

ABSTRACT

The most irradiated transiting hot Jupiters are characterized by anomalously inflated radii, sometimes exceeding Jupiter’s size by more than 60%. While different theoretical explanations have been applied, none of them provide a universal resolution to this observation, despite significant progress in the past years. We refine the photometric transit light curve analysis of 115 *Kepler* giant planet candidates based on public Q0–Q2 photometry. We find that 14% of them are likely false positives, based on their secondary eclipse depth. We report on planet radii versus stellar flux. We find an increase in planet radii with increased stellar irradiation for the *Kepler* giant planet candidates, in good agreement with existing hot Jupiter systems. We find that in the case of modest irradiation received from the stellar host, giant planets do not have inflated radii, and appear to have radii independent of the host star incident flux. This finding suggests that the physical mechanisms inflating hot Jupiters become ineffective below a given orbit-averaged stellar irradiation level of $\sim 2 \times 10^8 \text{ erg s}^{-1} \text{ cm}^{-2}$.

Key words: planetary systems – techniques: photometric

Online-only material: color figure

1. INTRODUCTION

The onset of giant exoplanet transit science, initiated by the discovery of HD 209458 b (Charbonneau et al. 2000; Henry et al. 2000), immediately revealed unexpected anomalous radii for several hot Jupiters. The so-called inflated radii became common as new transiting hot Jupiters were discovered. The anomalous giant planet radii were unexpected because in the mass regime of giant planets, the mass–radius relationship for giant planets was expected to be unique (Zapolsky & Salpeter 1969), assuming a given composition. Moreover, the compensating effects of electron degeneracy and electrostatic contribution from the classical ions yield a quasi-constant radius around 1 and $7 M_{\text{Jup}}$ (see, e.g., Chabrier et al. 2009). Soon after the discovery of 51 Peg b (Mayor & Queloz 1995), Guillot et al. (1996) correctly pointed out that strongly irradiated giant planets do not follow the same mass–radius relationship as isolated objects.

More than 100 known transiting hot Jupiters later, planet radius discrepancies are still common (e.g., Liu et al. 2008; Baraffe et al. 2010; Fortney et al. 2010; Ibgui et al. 2010). Despite numerous theoretical studies (see, e.g., Fortney & Nettelmann 2010 for a review), no universal mechanism seems to fully account for the observed radius anomalies.

The motivation of the present work is that most of the proposed mechanisms to explain inflated radii are expected to become less effective as the stellar incident flux decreases (e.g., Burrows et al. 2007; Fortney et al. 2007). We therefore study a *Kepler* subsample of 138 giant planet candidates to better understand the effect of irradiation across a wide range of orbital separation on giant extrasolar planet radii. We further note that transiting giant planets receiving modest stellar irradiation are particularly important for the derivation of their internal structure and composition, as the interior energy source is expected to affect the planetary radius only nominally (Miller & Fortney 2011).

The paper is organized as follows. We first describe in Section 2 how the sample of giant planet candidates was chosen. Then we present the data analysis that refined the system parameters and provided constraints on planethood of the candidates. The results of this analysis are then shown in Section 3. We finally discuss the behavior of the *Kepler* giant planet candidates in the radii versus stellar incident flux plane and estimate the *Kepler* false positive rate for this class of objects in Section 4.

2. DATA ANALYSIS

2.1. Selection of Giant Planet Candidates

This study is based on quarters Q0, Q1 and Q2 *Kepler* data that were publicly released on 2011 February 1 (Borucki et al. 2011). In total, the data sets encompass 136 days of photometric monitoring between 2009 May and September.

A list of 1235 *Kepler* Objects of Interest (KOI) was released, unveiling a huge diversity of exoplanet candidates in terms of planetary radii and orbital periods. One of the key elements of this release is the relatively low occurrence of Jupiter-sized candidates (see, e.g., Howard et al. 2011). Out of the 1235 planet candidates, only about 15% have radii above $0.6 R_{\text{Jup}}$, a result that supports the low frequency of giant planets found in radial velocity (RV) surveys (e.g., Howard et al. 2010), albeit for a different stellar population.

Our primary selection criterion is the planetary radius. Borucki et al. (2011) announced 165 giant planet candidates with $6 R_{\oplus} < R_p < 15 R_{\oplus}$ and 19 candidates with $15 R_{\oplus} < R_p < 22 R_{\oplus}$ for a total of 184 objects. We further restricted this sample to keep only “giant” planet candidates, defined here by $8 R_{\oplus} < R_p < 22 R_{\oplus}$. This step yielded 138 candidates. We removed the 14 KOI that have only one transit in Q0–Q2 and 9 other classified as “moderate” candidates, likely false positives, that exhibit centroid motion or difference of depth between odd and even transits (Batalha et al. 2010). This selection left us with a sample of 115 giant planet candidates.

2.2. Method

For each of the 115 KOI, we retrieved the Q0–Q2 raw long-cadence photometry (Jenkins et al. 2010a) from the Multimission Archive at STScI (MAST).¹ These data include all photometry in the form of individual light curves. We used the raw photometry instead of the Kepler-corrected (pre-search data conditioning; Jenkins et al. 2010b) photometry so that we could identify systematics on specific timescales as necessary input to our analysis. Moreover, by using the raw data we can assess the amplitude of correlated noise (from instrumental systematics and stellar variability combined) to derive uncertainties on stellar and planetary parameters.

To better characterize the 115 planet candidates, we performed individual Markov Chain Monte Carlo (MCMC) analysis for each KOI. The aim of this analysis was two-fold. The first goal was to remove false positives by way of detecting a robust secondary eclipse signal indicative of a stellar companion instead of a planetary companion. The second goal was to derive the stellar density from the transit light curve in order to further derive the stellar parameters and planetary radius. This step also required use of the stellar T_{eff} values drawn from the *Kepler* Input Catalog (KIC; Brown et al. 2011).

We used the implementation of the MCMC algorithm presented in Gillon et al. (2009, 2010) in order to derive the stellar and planetary parameters. MCMC is a Bayesian inference method that is based on stochastic simulations and that samples the posterior probability distributions of adjusted parameters for a given model. Our MCMC implementation uses the Gibbs sampler and the Metropolis–Hastings algorithm to estimate the posterior distribution function of all jump parameters. Our nominal model is based on a star and a transiting planet on a Keplerian orbit about their center of mass.

Input data provided to each MCMC consisted of the Q0–Q2 *Kepler* photometry and the KIC stellar T_{eff} value relevant to each candidate. Two runs were performed, each of them made of two Markov chains of 50,000 steps each. The purpose of the first run was to estimate the level of correlated noise in each light curve and to provide the second run with updated error bars on the jump parameters. In the second MCMC, the good mixing and convergence of the Markov chains were assessed using the Gelman–Rubin statistic criterion (Gelman & Rubin 1992).

We divided the total light curve in chunks of duration of ~ 24 to 48 hr and fitted for each of them the smooth photometric variations due to stellar variability or instrumental systematic effects with a time-dependent quadratic polynomial. Baseline model coefficients were determined at each step of the MCMC for each light curve with the singular value decomposition method (Press et al. 1992). The resulting coefficients were then used to correct the raw photometric light curves.

For each chunk of data, correlated noise was accounted for following Winn et al. (2008) and Gillon et al. (2010) to ensure reliable error bars on the fitted parameters. For this purpose, we compute a scaling factor based on the standard deviation of the binned residuals for each light curve with different time bins. The error bars are then multiplied by this scaling factor.

The rest of the important inputs for the MCMC are as follows. For each quarter, we estimated the degree of photometric dilution by using the contamination factor² computed from the KIC crowding matrix (Bryson et al. 2010) and then applied it to the transit photometry.

We assumed a quadratic law for the limb darkening and used $c_1 = 2u_1 + u_2$ and $c_2 = u_1 - 2u_2$ as jump parameters, where u_1 and u_2 are the quadratic coefficients. u_1 and u_2 were drawn from the theoretical tables of Claret & Bloemen (2011) for the corresponding KIC T_{eff} and $\log g$ values.

The MCMC has the following set of jump parameters: the planet/star flux ratio, the impact parameter b , the transit duration from first to fourth contact, the time of minimum light T_0 , the orbital period, the occultation depth, the two limb darkening (LD) combinations c_1 and c_2 , and the two parameters $\sqrt{e} \cos \omega$ and $\sqrt{e} \sin \omega$. A uniform prior distribution is assumed for all jump parameters but for c_1 and c_2 , for which a normal prior distribution is used, based on theoretical tables.

2.3. False Positive Assessment via Secondary Eclipses

The *Kepler* giant planet candidate list is not guaranteed against false positives, although a ranking of preliminary assessment is provided on MAST. Yet it is the false positive rate contributed by eclipsing binary stars with larger radii than Jupiter’s that would contaminate our findings. Furthermore, late type M dwarfs could actually produce planet-to-star area ratio indistinguishable from bona fide giant planets because of their similar radii to Jupiter-like objects (see, e.g., Chabrier et al. 2009). Obtaining radial-velocity measurements at orbital quadrature for more than 100 giant planet candidate objects is unrealistic for the purpose of the present study, given the faint V magnitude of the host stars and the number of targets of higher priority in the *Kepler* follow-up program.

We therefore used our MCMC method to search for a secondary eclipse whose depth would be indicative of a stellar companion instead of a planet. No constraint on the eccentricity was imposed since binaries with orbital periods of a few days only and eccentricity $e > 0.2$ are not uncommon (see, e.g., Rucinski et al. 2007; Maceroni et al. 2009).

We used the derived occultation depth F_P/F_* to compute the corresponding geometric albedo $A_g = (F_P/F_*)/(a^2/R_p^2)$ and the brightness temperature to assess the nature of each KOI. We further visually inspected the individual folded light curves, as discontinuities due to spacecraft roll, change of focus, pointing offsets, or safe mode events could create artifacts in the raw photometry and affect the detection of shallow features in the light curve. We present the results of this analysis, in terms of false positive rate, in Section 3.

2.4. Stellar Parameters

The photometric calibration of the *Kepler* field target stars presented in the KIC yields stellar radii uncertainties of 35% rms (Brown et al. 2011). Because the stellar radius uncertainty translates directly to a planet candidate size, the stellar radius uncertainty is too large for any useful constraint on the behavior of planetary radii with incident stellar flux and orbital distance. Hence, this motivated us to derive our own stellar radii by a different method than assuming the KIC stellar radii, which yields smaller uncertainties (of $\sim 15\%$ rms) on the derived stellar radius (see Section 3).

The method we use employs the empirical calibration law presented in Torres et al. (2010). The authors show that accurate stellar masses and radii could be deduced from the stellar effective temperature T_{eff} , surface gravity $\log g$, and metallicity [Fe/H] derived from spectroscopy. For this purpose they build a calibration law based on a large sample of well-characterized detached binaries. A linear regression algorithm then provides the stellar mass as a function of the spectroscopic parameters.

¹ <http://archive.stsci.edu/kepler/>

² Contamination values can be found in the fits files headers.

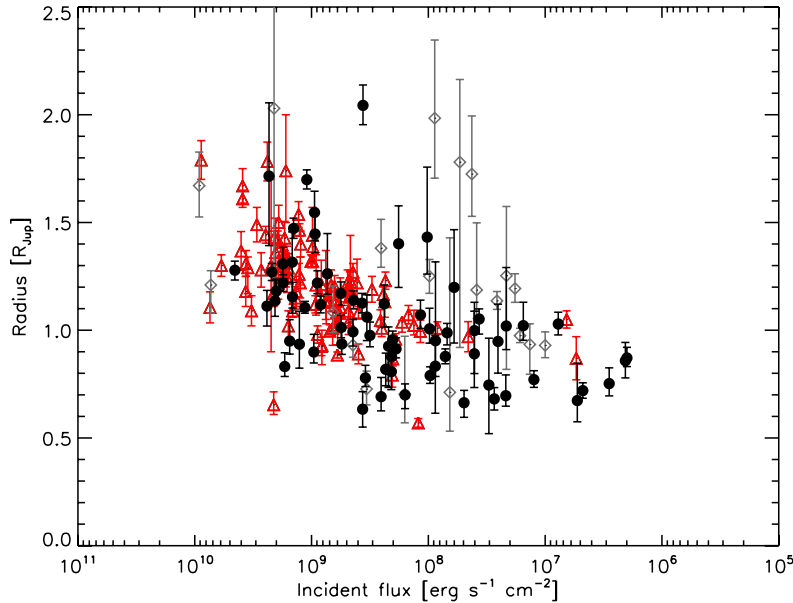


Figure 1. Planetary radii as a function of incident flux. The black filled circles are KOI ranked as planetary candidates in the frame of this work while gray diamonds represent KOI whose origin is ambiguous (see Section 3). Transiting giant planets previously published, and mostly from ground-based surveys, are shown as red triangles. The relevant parameters R_p , R_s , T_{eff} , and a have been drawn from <http://www.inscience.ch/transits> on 2011 August 29.

(A color version of this figure is available in the online journal.)

Enoch et al. (2010) further suggested to use as input the stellar density ρ_* instead of the stellar surface gravity $\log g$. The advantage of this approach is that the stellar density is well constrained by the transit light curve photometry (Seager & Mallén-Ornelas 2003), yielding better results than using the surface gravity derived from the spectroscopic analysis.

The empirical calibration implemented in the MCMC is therefore a function of T_{eff} , ρ_* , and the stellar metallicity $[\text{Fe}/\text{H}]$, which is poorly constrained from the KIC photometry (Brown et al. 2011). We thus imposed a 0.3 dex uncertainty on the stellar metallicity. At each step of the MCMC, ρ_* (deduced from the jump parameters), T_{eff} , and $[\text{Fe}/\text{H}]$ (drawn from the normal distribution based on the KIC value with the error bars quoted above) are used as input to the calibration law. The physical parameters of the system are then deduced using the resulting stellar mass. The intrinsic uncertainty of the parameters of the calibration relationship is accounted for by randomly drawing the parameter values from the normal distribution presented in Torres et al. (2010) at each iteration of the MCMC. The remainder of the uncertainty on the stellar radius is then mostly dominated by the error on the KIC T_{eff} and on the intrinsic scatter of the empirical relationship.

This method makes the derivation of the stellar mass possible at each step of the MCMC without the need of performing a separate analysis based on stellar evolution models.

3. RESULTS

The main result of this study is that giant planet candidate radii are independent of stellar incident flux below an incident flux of about $2 \times 10^8 \text{ erg s}^{-1} \text{ cm}^{-2}$ (Figure 1). Although the giant planet radius trend was hinted with published giant planets alone (Miller & Fortney 2011; Schneider et al. 2011; see also Figure 1) and theoretically expected (e.g., Fortney et al. 2007), inclusion of these new *Kepler* giant planet candidate radii yields a robust trend.

The objects supporting this result are the *Kepler* giant planet candidates that have no or shallow secondary eclipses consistent

with their equilibrium temperature at 2σ level or less. For comparison we include transiting planets not discovered by *Kepler* that overlap perfectly in the R_{planet} versus incident flux plane, but mainly populate the high incident flux regime. The *Kepler* Q0–Q2 coverage not only enables almost a doubling of the transiting giant planet candidates but also extends the coverage out to lower incident fluxes as compared to currently known transiting planets.

Complicating the result is the fact that *Kepler* planet candidates are not vetted as actual planets. We have used our MCMC analysis to assess false positives via secondary eclipse detection. Indeed, 16 planet candidates show strong evidence for deep secondary eclipses suggesting a 4σ discrepancy or more with their estimated equilibrium temperature. Such objects are discarded from the study. Finally, 22 planet candidates yield a secondary eclipse signature whose origin cannot be secured, the inferred brightness temperature being consistent with either a planetary or stellar companion. We still choose to include those candidates in Figure 1 with distinct symbols. Additional data will help in tightening the nature of those objects.

We notice that eclipsing binaries with grazing transits combined to non-zero orbital eccentricity would not yield any secondary eclipse and would therefore be wrongly identified as planets in our study. Any such contamination should be uniform with the range of incident fluxes explored in this study and would not affect the main finding of a trend in giant planet radii.

For most of our planet candidates, there is no information about the orbital eccentricity. Instead of unrealistically assuming circular orbits, we assigned each candidate an eccentricity value drawn from the distribution presented in Wang & Ford (2011), as well as a random value for the argument of periastron. This approach is reasonable since no significant trend seems to exist between eccentricity and orbital period for *Kepler* candidates (Moorhead et al. 2011).

To gauge the impact of orbital eccentricity on our results, we performed a new MCMC analysis by imposing priors on $\sqrt{e} \sin \omega$ and $\sqrt{e} \cos \omega$ (see Section 2.2), based on the values

Table 1
List of KOI Used in This Study

Planetary	Planetary (continued)	Ambiguous	False Positives
1.01	398.01	12.01	194.01
2.01	410.01	187.01	197.01
10.01	417.01	189.01	208.01
17.01	418.01	458.01	552.01
18.01	421.01	617.01	609.01
20.01	423.01	728.01	743.01
22.01	425.01	763.01	745.01
94.01	625.01	767.01	779.01
97.01	674.01	772.01	876.01
98.01	686.01	823.01	895.01
100.01	698.01	840.01	1003.01
127.01	760.01	855.01	1152.01
128.01	801.01	856.01	1177.01
135.01	805.01	918.01	1540.01
138.01	806.01	929.01	1541.01
183.01	806.02	960.01	1543.01
186.01	809.01	961.02	
188.01	815.01	961.03	
190.01	824.01	1020.01	
191.01	846.01	1285.01	
192.01	850.01	1299.01	
193.01	858.01	1385.01	
195.01	871.01		
196.01	882.01		
199.01	883.01		
202.01	889.01		
203.01	897.01		
205.01	908.01		
214.01	913.01		
217.01	931.01		
254.01	1089.01		
351.01	1176.01		
366.01	1227.01		
368.01	1391.01		
372.01	1486.01		

Notes. KOI meeting our criteria (see Section 3) are shown in the “planetary” column while the probable stellar companions are shown in the “false positives” column. The intermediate class is shown under “ambiguous.”

drawn for e and ω in the previous step. We then computed the orbit-averaged incident flux for each candidate and found an excellent agreement (4% on average) with the fluxes obtained for the circular case. The reported trend in the R_p versus incident flux plane is therefore robust to the planetary candidates’ orbital eccentricity. We show our results (assuming the eccentricity distribution described above) in Figure 1.

In summary, out of the 115 KOI, 70 of them exhibit no or shallow secondary eclipses consistent with their equilibrium temperature. Those objects are therefore considered to be of planetary origin, whereas 16 are identified as stellar companions and 22 are of ambiguous classification. We list the KOI and their identification in Table 1.

In the course of the analysis, seven KOI got their radius revised to less than $6 R_{\oplus}$. Those KOI were thus discarded from our study as no longer part of the giant planet candidate sample.

4. DISCUSSION

4.1. Giant Planet Radius Inflation Mechanisms

KOI classified as planetary candidates in the frame of this study yield planetary radii versus incident flux in good agreement with published transiting planet data, as shown in

Figure 1. Remarkably, this set of KOI results in constant radii of $\sim 0.87 \pm 0.12 R_J$,³ similar to Jupiter, below an incident flux of $\sim 2 \times 10^8 \text{ erg s}^{-1} \text{ cm}^{-2}$. We report no inflated giant planet radii below this threshold.

Several explanations have been invoked to bring or maintain heat in the planetary interiors, necessary to explain radii anomalies through a larger equilibrium radius. An exhaustive description can be found in, e.g., Fortney & Nettelmann (2010) and Baraffe et al. (2010) but none seem to reproduce all planets with inflated radii. The increase of temperature of the top layers of a giant planet caused by significant incident flux creates a shallow gradient of temperature deep in the atmosphere, close to an isothermal layer. This gradient slows down the loss of heat from the planet interior and thus the contraction (Guillot et al. 1996; Barman et al. 2001), as compared to planets receiving modest irradiation (Guillot & Showman 2002). This explanation however only reproduces inflated radii up to $\sim 1.2 R_{Jup}$ but cannot yield planet radii of $1.7 R_{Jup}$ or more that have been reported in the literature.

Tidal energy dissipation in the giant planet interior is expected to counteract the contraction (Bodenheimer et al. 2001). Bodenheimer et al. (2003) proposed that an additional companion in the system could pump the planet eccentricity that would be dissipated through tides. Significant follow-up on this possibility emerged in the last years. Levrard et al. (2009) have for instance shown that most known transiting planets were spiraling toward their star due to tidal dissipation. Miller et al. (2009) modeled coupled thermal evolution and tidal effects on giant planets and were able to reproduce the radius anomalies for 35 out of 45 planet parts of their sample, assuming ad hoc initial conditions. It has been recently shown by Arras & Socrates (2010) that the inclusion of thermal tide effects allows further gravitational tidal dissipation during the circularized, equilibrium state, thus producing larger radius excesses than gravitational tidal friction alone.

Electrical current generated through the interaction of ionized particles with the planetary magnetic field causes a dissipation of energy in the planetary interior (Batygin & Stevenson 2010; Perna et al. 2010). Laughlin et al. (2011) find support for this hypothesis from the set of transiting planets known in 2010 but also state that other processes should be contributing to account for the observed anomalies, such as the effects of heavy element abundances (Batygin et al. 2011) or the internal heating induced by tidal circularization for eccentric planets.

Layered convection should occur in atmospheres characterized by molecular weight gradients (Chabrier & Baraffe 2007). This would decrease the loss of heat and slow down the contraction in the planetary interiors. This mechanism is independent of the incident stellar flux.

Our results suggest that the combinations of mechanisms responsible for the giant planet inflated radii are correlated to the strength of the stellar incident flux.

For the most close-in planetary candidates, tidal effects could contribute significantly and add to the sole incidence of stellar irradiation.

As part of this study, we find no support for a process that would be solely based on layered convection as no cold inflated planets are reported.

There is observed scatter in the plateau of giant planet radii below $\sim 2 \times 10^8 \text{ erg s}^{-1} \text{ cm}^{-2}$. We speculate this scatter could

³ Jupiter radius itself is $0.977 R_J$ when using its mean radius of 69,894 km instead of its equatorial radius of 71,492 km (see Table 1 of Guillot 2005)

be due to the effects of metallicity. Planets enriched with heavy elements yield a more compact structure, and thus a smaller radius, like HD 149026 b (Sato et al. 2005).

4.2. False Positive Rate

A by-product of our MCMC analysis is also an important result: an estimated false positive rate for the *Kepler* giant planet candidate listing. According to our analysis, 14% of the *Kepler* giant planet candidates studied in this sample are eclipsing binaries or background eclipsing binaries. This result is based on identification of large discrepancy between the candidate's equilibrium temperature and its measured brightness temperature in the *Kepler* band pass. We further note that the 14% false positive rate number might even be higher in the case of grazing events or eccentric orbits, for which the detection of a secondary eclipse is not possible. We found no false positives among the 10 multi-planetary systems included in our sample.

Additional *Kepler* data will allow an extension of the present study to planets with longer orbits than the candidates presented in this work. The next quarters of *Kepler* photometry will also help in tightening the exact fraction of false positives among giant planet candidates by improving the characterization of secondary eclipses.

In summary, this work presents one of the first results from the emerging science of exoplanet statistics enabled by *Kepler*'s exquisite photometry and large pool of planet candidates. With future *Kepler* data, we expect many other planet population trends to be identified and to weigh in or solve key exoplanet questions.

We are grateful to Jonathan Fortney, Jack Lissauer, Eric Ford, and Jérémy Leconte for insightful comments that improved this manuscript. We warmly thank Michaël Gillon for sharing his expertise on MCMC methods. We thank the *Kepler* Giant Planet Working Group for useful discussions and especially Jason Rowe and Jon Jenkins for their invaluable inputs regarding *Kepler* photometry. We thank the anonymous referee for a helpful review that improved this manuscript. Funding for the *Kepler* mission is provided by the National Aeronautics and Space Administration (NASA) Science Mission Directorate. This work was funded in part by the Kepler Participating Science Program grant NNX08BA51G.

Facility: *Kepler*

REFERENCES

- Arras, P., & Socrates, A. 2010, *ApJ*, 714, 1
- Baraffe, I., Chabrier, G., & Barman, T. 2010, *Rep. Prog. Phys.*, 73, 016901
- Barman, T. S., Hauschildt, P. H., & Allard, F. 2001, *ApJ*, 556, 885
- Batalha, N. M., Rowe, J. F., Gilliland, R. L., et al. 2010, *ApJ*, 713, L103
- Batygin, K., & Stevenson, D. J. 2010, *ApJ*, 714, L238
- Batygin, K., Stevenson, D. J., & Bodenheimer, P. H. 2011, *ApJ*, 738, 1
- Bodenheimer, P., Laughlin, G., & Lin, D. N. C. 2003, *ApJ*, 592, 555
- Bodenheimer, P., Lin, D. N. C., & Mardling, R. A. 2001, *ApJ*, 548, 466
- Borucki, W. J., Koch, D. G., Basri, G., et al. 2011, *ApJ*, 736, 19
- Brown, T. M., Latham, D. W., Everett, M. E., & Esquerdo, G. A. 2011, *AJ*, 142, 112
- Bryson, S. T., Tenenbaum, P., Jenkins, J. M., et al. 2010, *ApJ*, 713, L97
- Burrows, A., Hubeny, I., Budaj, J., & Hubbard, W. B. 2007, *ApJ*, 661, 502
- Chabrier, G., & Baraffe, I. 2007, *ApJ*, 661, L81
- Chabrier, G., Baraffe, I., Leconte, J., Gallardo, J., & Barman, T. 2009, in AIP Conf. Ser. 1094, *Cool Stars, Stellar Systems and the Sun*, ed. E. Stempels (Melville, NY: AIP), 102
- Charbonneau, D., Brown, T. M., Latham, D. W., & Mayor, M. 2000, *ApJ*, 529, L45
- Claret, A., & Bloemen, S. 2011, *A&A*, 529, A75
- Enoch, B., Collier Cameron, A., Parley, N. R., & Hebb, L. 2010, *A&A*, 516, A33
- Fortney, J. J., Baraffe, I., & Militzer, B. 2010, in *Exoplanets*, ed. S. Seager (Tucson, AZ: Univ. Arizona Press), 397
- Fortney, J. J., Marley, M. S., & Barnes, J. W. 2007, *ApJ*, 659, 1661
- Fortney, J. J., & Nettelmann, N. 2010, *Space Sci. Rev.*, 152, 423
- Gelman, A., & Rubin, D. B. 1992, *Stat. Sci.*, 7, 457
- Gillon, M., Demory, B.-O., Triaud, A. H. M. J., et al. 2009, *A&A*, 506, 359
- Gillon, M., Lanotte, A. A., Barman, T., et al. 2010, *A&A*, 511, A3
- Guillot, T. 2005, *Ann. Rev. Earth Planet. Sci.*, 33, 493
- Guillot, T., Burrows, A., Hubbard, W. B., Lunine, J. I., & Saumon, D. 1996, *ApJ*, 459, L35
- Guillot, T., & Showman, A. P. 2002, *A&A*, 385, 156
- Henry, G. W., Marcy, G. W., Butler, R. P., & Vogt, S. S. 2000, *ApJ*, 529, L41
- Howard, A. W., Marcy, G. W., Bryson, S. T., et al. 2011, *ApJ*, submitted (arXiv:1103.2541)
- Howard, A. W., Marcy, G. W., Johnson, J. A., et al. 2010, *Science*, 330, 653
- Ibguí, L., Burrows, A., & Spiegel, D. S. 2010, *ApJ*, 713, 751
- Jenkins, J. M., Caldwell, D. A., Chandrasekaran, H., et al. 2010a, *ApJ*, 713, L120
- Jenkins, J. M., Caldwell, D. A., Chandrasekaran, H., et al. 2010b, *ApJ*, 713, L87
- Laughlin, G., Crismani, M., & Adams, F. C. 2011, *ApJ*, 729, L7
- Levrard, B., Winisdoerffer, C., & Chabrier, G. 2009, *ApJ*, 692, L9
- Liu, X., Burrows, A., & Ibguí, L. 2008, *ApJ*, 687, 1191
- Maceroni, C., Montalbán, J., Michel, E., et al. 2009, *A&A*, 508, 1375
- Mayor, M., & Queloz, D. 1995, *Nature*, 378, 355
- Miller, N., & Fortney, J. J. 2011, *ApJ*, 736, L29
- Miller, N., Fortney, J. J., & Jackson, B. 2009, *ApJ*, 702, 1413
- Moorhead, A. V., Ford, E. B., Morehead, R. C., et al. 2011, *ApJS*, 197, 1
- Perna, R., Menou, K., & Rauscher, E. 2010, *ApJ*, 724, 313
- Press, W. H., Teukolsky, S. A., Vetterling, W. T., & Flannery, B. P. 1992, *Numerical Recipes in FORTRAN. The Art of Scientific Computing* (2nd ed.; Cambridge: Cambridge Univ. Press)
- Rucinski, S. M., Kuschnig, R., Matthews, J. M., et al. 2007, *MNRAS*, 380, L63
- Sato, B., Fischer, D. A., Henry, G. W., et al. 2005, *ApJ*, 633, 465
- Schneider, J., Dedieu, C., Le Sidaner, P., Savalle, R., & Zolotukhin, I. 2011, *A&A*, 532, A79
- Seager, S., & Mallén-Ornelas, G. 2003, *ApJ*, 585, 1038
- Torres, G., Andersen, J., & Giménez, A. 2010, *A&AR*, 18, 67
- Wang, J., & Ford, E. B. 2011, *MNRAS*, 1590
- Winn, J. N., Holman, M. J., Torres, G., et al. 2008, *ApJ*, 683, 1076
- Zapolsky, H. S., & Salpeter, E. E. 1969, *ApJ*, 158, 809